In-phase and quadrature frequency-shift keying for low-power optical wireless communications

Ali Waqar Azim, Yannis Le Guennec, Laurent Ros

In-phase and Quadrature Frequency-Shift Keying for Low-Power Optical Wireless Communications

Ali Waqar Azim, Yannis Le Guennec, Laurent Ros

Abstract

This article proposes using in-phase and quadrature frequency-shift keying (IQFSK) modulation for low-power optical wireless communications (OWC). IQFSK independently leverages both cosine and sine basis functions to enhance the system's spectral efficiency (SE). It uses only the odd harmonic frequencies for these basis functions, allowing the clipping of negative amplitude excursions without losing information, making the waveform compatible with OWC. The work presents optimal maximum likelihood and low-complexity sub-optimal detection mechanisms for IQFSK. The proposed scheme is analyzed analytically and with numerical simulations. The simulation and analytical results indicate that the proposed scheme is more energy-efficient, can attain a better energy and SE trade-off by exploiting the frame structure of the waveform, and has a lower minimum squared Euclidean distance relative to other state-of-the-art FSK-based counterparts, thus establishing it as one of the most efficient FSK approaches for low-power OWCs.

Index Terms

Frequency-shift keying, intensity modulation and direct-detection, spectral efficiency, energy efficiency, coherent detection, non-coherent detection, modulation and coding.

I. INTRODUCTION

In emerging wireless standards, seamless communication between connected devices at low power is crucial [1]. However, the limited availability of radio-frequency (RF) spectral resources poses practical challenges when deploying these low-power communication systems. One potential solution is incorporating optical wireless communications (OWC) alongside RF ones. This approach necessitates developing low-power waveform designs compatible with intensity modulation and direct-detection (IM-DD) implementation. However, the current state-of-the-art offers only a few protocols that fulfill these requirements, and most are not optimized for energy and spectral efficiency (SE).

Low-power applications can use waveforms from either the linear or orthogonal categories [2]. Linear modulations include on-off keying (OOK) and pulse amplitude modulation (PAM). OOK is straightforward

Ali Waqar Azim is with Engineering Division, New York University Abu Dhabi, Saadiyat Island, P.O. Box 129188, Abu Dhabi, United Arab Emirates (email: aliwaqarazim@gmail.com).

Yannis Le Guennec and Laurent Ros are with Université Grenoble Alpes, CNRS, Grenoble INP, GIPSA-Lab, Grenoble, 38000, France (email: {yannis.leguennec,laurent.ros}@gipsa-lab.grenoble-inp.fr).

to implement through IM-DD, but it falls short compared to orthogonal modulations regarding energy efficiency (EE) [2]. On the other hand, PAM is not optimized for low-power applications because increasing the alphabet cardinality improves the SE but negatively affects the resulting EE. Consequently, linear modulations are not suitable for low-power applications.

In contrast, orthogonal modulations have been recognized as superior waveform designs, particularly for low-power applications. Unlike linear modulations like PAM, orthogonal modulations' EE improves as the alphabet cardinality increases. Notable examples of suitable orthogonal modulations include pulse-position modulation (PPM) and IM-DD-compatible frequency-shift keying (FSK) variants [3], [4]. However, PPM suffers from limitations such as a high peak-to-average power ratio, increased sensitivity to multipath propagation, and potential receiver synchronization issues [5], [6]. Consequently, waveform designs based on FSK are preferred as they successfully circumvent these limitations.

Since conventional FSK schemes are incompatible with IM-DD implementation due to their bipolar and complex-valued nature, numerous IM-DD-compatible FSK schemes have been proposed in the literature. These include direct-current FSK (DCFSK) [2], [7], unipolar-FSK (UFSK) [2], DC-frequency and phase-shift keying (DCFPSK) [8], asymmetrically clipped FSK (ACFSK) [9], asymmetric FSK [10], and OOK-M-FSK [11]. In DCFSK, a real-valued waveform is achieved by exploiting the Hermitian symmetry (HS) property of discrete Fourier transform (DFT), while non-negativity is obtained by adding a DC bias to the bipolar waveform. However, adding a DC bias significantly degrades the EE of the resulting waveform. This issue is addressed by UFSK, where positive amplitude excursions and sign-flipped negative amplitude excursions are transmitted in two consecutive time frames, resulting in better EE at the cost of lower SE. ACFSK uses only odd frequency tones to achieve an anti-symmetric waveform, allowing negative amplitudes to be clipped without losing information. ACFSK performs better than DCFSK and marginally better than UFSK in terms of EE, although its SE performance is the same as that of UFSK, which is half that of DCFSK. DCFPSK scheme enhances the DFSK scheme by incorporating PSK alphabets to improve SE. It has been demonstrated that the optimal variant of DCFPSK increases the SE of conventional FSK by 2 bits, but it cannot avoid the limitation of using a DC bias, leading to lower EE. Other variants, such as asymmetric FSK and OOK-M-FSK, also have their limitations, which are not straightforward to overcome. Notably, all these schemes use either cosine or cosine/sine basis with the same single frequency for the in-phase/quadrature channel, leading to inefficient waveform designs. Thus, it can be concluded that designing an FSK waveform involves balancing the trade-off between SE and EE, fundamentally determined by the waveform's frame structure, which can be improved by exploiting both the cosine and sine basis functions.

Against the given background, the main hypothesis behind this work is to explore efficient FSK-

based waveform design for OWC by efficiently exploiting both the cosine and the sine basis function simultaneously to simultaneously achieve spectral and energy efficiency. Thus, this article introduces in-phase and quadrature frequency-shift keying (IQFSK) as an alternative to the existing FSK-based techniques for low-power OWC. The contributions of this article are as follows:

1) A comprehensive elucidation of the frame structure for IQFSK is presented. The use of cosine and sine basis functions independently in IQFSK leads to a special dual-tone technique. Furthermore, IQFSK achieves non-negativity by clipping the time domain symbol without loss of information which is obtained by only using the odd frequencies for both cosine and sine basis functions [9]. To the best of our knowledge, this frame structure for the FSK-based approach has never been studied for low-data-rate OWC.

2) We demonstrate the feasibility of optimal maximum likelihood (ML) and sub-optimal low-complexity detection methods for the proposed scheme. This demonstrates that the proposed waveform design does not lead to complex signal processing at the receiver and the transmitted information can be recovered in a straightforward manner.

3) We derive mathematical expressions for the minimum squared Euclidean distance (MSED), which reveal that clipping leads to non-orthogonality and reduction of the MSED relative to conventional bipolar FSK between different symbols. It is shown that the proposed scheme has the highest MSED relative to other FSK variants for OWC, leading to better overall performance.

4) We perform comprehensive analytical and simulation analysis which establishes that IQFSK outperforms existing alternatives in terms of both SE and EE trade-off.

The remainder of this article is structured as follows. Section II examines IQFSK waveform design and detection, Section III and Section IV presents analytical and simulation results, respectively, and conclusions are provided in Section V.

II. IQFSK WAVEFORM GENERATION AND DETECTION

In this section, we elucidate waveform generation and the detection mechanisms for IQFSK.

A. Waveform Generation

Let B be the single-sided baseband bandwidth of the transmitted symbol, and T_{s} the symbol duration. M frequencies spaced by $\Delta f = 1/T_{\mathrm{s}}$ can be defined in $[-B; B]$, implying that $B = (M/2)\Delta f = M/2T_{\mathrm{s}}$. It is important to note that through M-order DFT, we can generate M complex orthogonal symbols within $[-B; B]$. The requirement to uphold HS, however, restricts us to generating only $M/2 - 1$ orthogonal real-valued bipolar symbols while operating within the same bandwidth [2], [7]. In IQFSK, generating
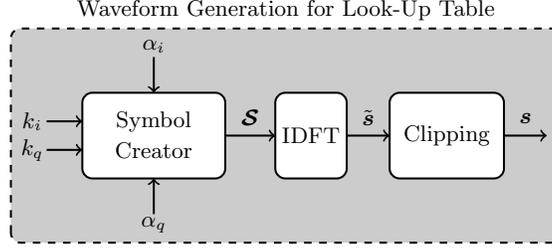
Fig. 1: Look-up Table creation for all the possible IQFSK waveforms.

asymmetric bipolar symbols enables us to clip the negative amplitude excursions and produce non-negative symbols; reducing the usable frequency elements to $M/4$ for both the in-phase and the quadrature components. Note that the asymmetric bipolar symbols can be generated using only the odd frequency tones for both in-phase and quadrature components. The IQFSK time-domain symbol, $s(t)$, having the k_i-th activated frequency for the cosine basis (in-phase component) and the k_q activated frequency for the sine basis (quadrature component) is given as (cf. [9] for clipping impact):

$$s(t) = \underbrace{\alpha_i \cos\left(2\pi k_i \Delta f t\right) - \alpha_q \sin\left(2\pi k_q \Delta f t\right)}_{\text{Signal}} + \underbrace{\left|\alpha_i \cos\left(2\pi k_i \Delta f t\right) - \alpha_q \sin\left(2\pi k_q \Delta f t\right)\right|}_{\text{Clipping Distortion}}, \tag{1}$$

for $t \in [0, T_\text{s}]$, where $\{\alpha_i, \alpha_q\} \in \{-1, 1\}$ are the possible amplitudes for the in-phase and the quadrature components, and $|\cdot|$ is the absolute operator. As aforementioned, only the odd frequencies are used for the in-phase and the quadrature components (to avoid information loss during the clipping process), implying $\{k_i, k_q\} \in \{1, 3, \cdots, M/2 - 1\}$. Given the symbols structure of IQFSK (cf. (1)), the electrical symbol energy, $E_{\text{s(elec)}}$, evaluates to:

$$E_{\text{s(elec)}} = \int_0^{T_\text{s}} s^2(t)\mathrm{d}t = \left(\alpha_i^2 + \alpha_q^2\right) T_\text{s}, \quad \forall\{k_i, k_q\}. \tag{2}$$

B. Look-Up Table Creation

By considering different combinations of α_i, k_i, α_q, and k_q, a dictionary, $\mathcal{D}$ of IQFSK symbols having a cardinality of $|\mathcal{D}| = M^2/4$ (possible symbols for a given M) can be generated as illustrated in Fig. 1. It may be noticed that the binary-to-decimal conversion of $\{\lambda_{\alpha_i}, \lambda_{\alpha_q}\} = \log_2(2)$ and $\{\lambda_i, \lambda_q\} = \log_2(M/4)$ bits determines α_i, α_q, k_i, and k_q. The M available frequencies in $[-B; B]$ are $\tilde{k} = [\![-M/2, M/2 - 1]\!]$. The 0th and the $-M/2$th frequency components are null, in order not to use the DC component and maintain HS. k_i and k_q belong to the odd positive frequencies among $k = [\![1, M/2 - 1]\!]$. In contrast, the negative frequencies are used for HS. This symbol structure in the frequency-domain leads to $\mathcal{S}$, which is a complex vector of cardinality $|\mathcal{S}| = M$ containing up to four non-zeros values, two for the real part and two for the imaginary part. The M-order inverse DFT (IDFT) of $\mathcal{S}$ leads to $\tilde{s}$, for which the
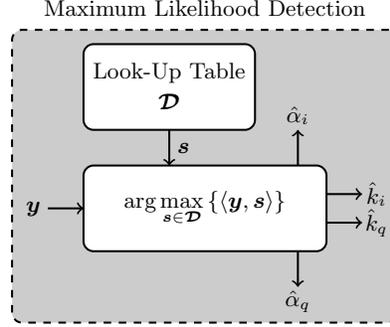
Fig. 2: Maximum likelihood detection for IQFSK.

negative amplitude excursions are clipped to zero to attain a unipolar (i.e., positive) IQFSK time-domain symbol, s. $\mathcal{D}$ is then interpolated into the look-up table.

C. Detection Mechanisms

This section covers the optimal ML and sub-optimal detection methods for IQFSK, along with a brief overview of the complexity of each mechanism.

1) Maximum Likelihood Detection: The ML criterion identifies $s \in \mathcal{D}$ that maximizes the likelihood function, $p(\boldsymbol{y}|\boldsymbol{s})$, where $\boldsymbol{y}$ is the received symbol. $p(\boldsymbol{y}|\boldsymbol{s})$ is the conditional probability of receiving $\boldsymbol{y}$ when $\boldsymbol{s}$ is sent. ML detection assumes that the probability of transmitting any IQFSK symbol in $\mathcal{D}$ is $p(\boldsymbol{s}) = 1/|\mathcal{D}|$ and that the electrical symbol energy of all IQFSK symbols is equal to $E_{\text{S(elec)}}$. The IQFSK parameters using ML detection are evaluated as:

$$\hat{k}_i, \hat{k}_q, \hat{\alpha}_i, \hat{\alpha}_q = \arg\max_{\boldsymbol{s} \in \mathcal{D}} \{p(\boldsymbol{y}|\boldsymbol{s})\} = \arg\max_{\boldsymbol{s} \in \mathcal{D}} \{\langle \boldsymbol{y}, \boldsymbol{s} \rangle\}, \tag{3}$$

Fig. 2 provides the system model for ML detection. The complexity of ML detection is $\mathcal{O}(M^2)$, which is high.

2) Low-Complexity Sub-Optimal Detection: Fig. 3 illustrates the low-complexity sub-optimal detector for IQFSK. In the detection process, $\boldsymbol{y}$ is subjected to DFT, which yields $\mathcal{Y}$. Afterwards, separating the in-phase and the quadrature components of $\mathcal{Y}$ results in $\Re\{\mathcal{Y}\}$ and $\Im\{\mathcal{Y}\}$, respectively, where $\Re\{\cdot\}$ and $\Im\{\cdot\}$ evaluates the real and imaginary component of a complex argument. The estimated frequencies of the in-phase and the quadrature components, $\hat{k}_i$, and $\hat{k}_q$, are determined as:

$$\hat{k}_i = \arg\max_{k \in k_i} \{|\Re\{\mathcal{Y}(k)\}|\}, \tag{4}$$

and

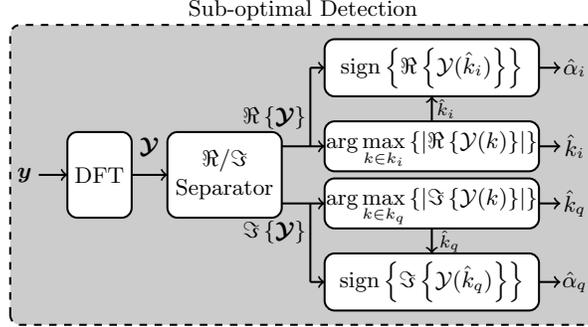$$\hat{k}_q = \arg\max_{k \in k_q} \{|\Im\{\mathcal{Y}(k)\}|\}, \tag{5}$$

Fig. 3: Low-complexity sub-optimal detection for IQFSK.

TABLE I: Characteristics of different IQFSK alternatives. Here, β is the bias used for DCFSK and DCFPSK, the symbol energy of each scheme is evaluated as $E_{\mathrm{s(elec)}} = \int_0^{T_\mathrm{s}} s^2(t)\mathrm{d}t$, M_φ is the number of phase shifts used for DCFPSK and ACFPSK, M is the size of DFT or discrete cosine transform (DCT), and η is the SE of each scheme.

Modulation	Transmit Symbol, $s(t)$	MSED, $d_{\min}^2$	SE, η
IQFSK	$\alpha_i \cos(2\pi k_i \Delta f t) - \alpha_q \sin(2\pi k_q \Delta f t)$ $+ \lvert \alpha_i \cos(2\pi k_i \Delta f t) - \alpha_q \sin(2\pi k_q \Delta f t)\rvert$	$0.6112 E_{\mathrm{s(elec)}}$	$\frac{4\log_2(M)}{M}$
DCFPSK [8]	$\alpha \cos(2\pi k \Delta f t + \varphi) + \beta$	$\nicefrac{2}{3} E_{\mathrm{s(elec)}}$ $(M_\varphi = 4)$	$\frac{2\log_2(M/2-1)+2\log_2(M_\varphi)}{M}$
ACFSK [9]	$\alpha \cos(2\pi k \Delta f t) + \lvert \alpha \cos(2\pi k \Delta f t)\rvert$	$(2 - \nicefrac{3\sqrt{3}}{2\pi}) E_{\mathrm{s(elec)}}$	$\frac{2\log_2(M/2)}{M}$
DCFSK [2]	$\alpha \cos(2\pi k \Delta f t) + \beta$	$\nicefrac{2}{3} E_{\mathrm{s(elec)}}$	$\frac{2\log_2(M)}{M}$

for $k = [\![1, \nicefrac{M}{2} - 1]\!]$. After determining $\hat{k}_i$, and $\hat{k}_q$, $\hat{\alpha}_i$, and $\hat{\alpha}_q$ are determined as:

$$\hat{\alpha}_i = \mathrm{sign}\left\{\Re\left\{\mathcal{Y}(\hat{k}_i)\right\}\right\}, \tag{6}$$

and

$$\hat{\alpha}_q = \mathrm{sign}\left\{\Im\left\{\mathcal{Y}(\hat{k}_q)\right\}\right\}, \tag{7}$$

respectively. The sub-optimal detector requires the computation of M-order DFT with a real-valued input. Considering that DFT is implemented via the Fast Fourier transform, the complexity of sub-optimal detection is $\mathcal{O}(M)$, which is significantly less than the complexity of the optimal ML detector.

III. THEORETICAL ANALYSIS OF IQFSK

In this section, we quantify the non-orthogonality of IQFSK symbols, and determine the MSED. We also examine the SE of IQFSK and compare it with other counterparts.

A. Orthogonality Analysis

To analytically determine the non-orthogonality of IQFSK symbols, we evaluate the inner product of $\boldsymbol{s}$ and $\tilde{\boldsymbol{s}}$, as $\langle \boldsymbol{s}, \tilde{\boldsymbol{s}}\rangle = \int_0^{T_\mathrm{s}} s(t)\tilde{s}(t)\mathrm{d}t$. For $s(t)$, we consider the following parameters, k_i, k_q, α_i, and α_q. In contrast, for $\tilde{s}(t)$, we consider $\tilde{k}_i, \tilde{k}_q, \tilde{\alpha}_i$, and $\tilde{\alpha}_q$. Note that the following conditions must hold to evaluate

$\langle \boldsymbol{s}, \tilde{\boldsymbol{s}} \rangle$: (i) $k_i \neq \tilde{k}_i$; and (ii) $k_q \neq \tilde{k}_i$. Moreover, α_i, α_q, $\tilde{\alpha}_i$, and $\tilde{\alpha}_q$ do not impact $\langle \boldsymbol{s}, \tilde{\boldsymbol{s}} \rangle$; therefore, it does not matter if they are the same or different. After some straightforward manipulations, $\langle \boldsymbol{s}, \tilde{\boldsymbol{s}} \rangle$ yields:

$$\langle \boldsymbol{s}, \tilde{\boldsymbol{s}} \rangle = \int_0^{T_{\mathrm{s}}} \left(|\alpha_i \cos\left(2\pi k_i \Delta ft\right) - \alpha_q \sin\left(2\pi k_q \Delta ft\right)| \ \ |\tilde{\alpha}_i \cos(2\pi \tilde{k}_i \Delta ft) - \tilde{\alpha}_q \sin(2\pi \tilde{k}_q \Delta ft)| \right) \mathrm{d}t. \tag{8}$$

From (8), it is readily identifiable that the IQFSK symbols are not orthogonal as $\langle \boldsymbol{s}, \tilde{\boldsymbol{s}} \rangle \neq 0$, and the cause of this loss of orthogonality is the clipping distortion generated by the IQFSK symbols.

B. Euclidean Distance Analysis

Assuming that the symbol energy of all possible IQFSK symbols is $E_{\mathrm{s_{(elec)}}}$, the Euclidean distance between any two IQFSK symbols $\boldsymbol{s}$, and $\tilde{\boldsymbol{s}}$, is evaluated as:

$$d^2 = \|\boldsymbol{s} - \tilde{\boldsymbol{s}}\|^2 = 2E_{\mathrm{s_{(elec)}}} - 2\langle \boldsymbol{s}, \tilde{\boldsymbol{s}} \rangle, \tag{9}$$

where $\| \cdot \|^2$ evaluates the Euclidean norm.

For orthogonal symbols (classical bipolar FSK), $\langle \boldsymbol{s}, \tilde{\boldsymbol{s}} \rangle = 0$; however, it is evident from (8) that this is not the case for IQFSK; thus, the distance between the two (real-valued non-negative) IQFSK symbols is expected to be less than $2E_{\mathrm{s_{(elec)}}}$. To specify the MSED for IQFSK symbols, we determine the two IQFSK symbols with the highest correlation, i.e., $\langle \boldsymbol{s}, \tilde{\boldsymbol{s}} \rangle_{\max}$. By evaluating the $\langle \boldsymbol{s}, \tilde{\boldsymbol{s}} \rangle$ for all the possible IQFSK symbols using different M, we determine that the two IQFSK symbols which exhibit $\langle \boldsymbol{s}, \tilde{\boldsymbol{s}} \rangle_{\max}$ have the following parameters. For $\boldsymbol{s}$, $\{\alpha_i, k_i, \alpha_q, k_q\} = \{1, 1, 1, 1\}$, and for $\tilde{\boldsymbol{s}}$, we have $\{\tilde{\alpha}_i, \tilde{k}_i, \tilde{\alpha}_q, \tilde{k}_q\} = \{1, 1, 1, 3\}$. Hence, $\langle \boldsymbol{s}, \tilde{\boldsymbol{s}} \rangle_{\max}$ equates to:

$$\langle \boldsymbol{s}, \tilde{\boldsymbol{s}} \rangle_{\max} = \int_0^{T_{\mathrm{s}}} \left(|\cos\left(2\pi\Delta ft\right) - \sin\left(2\pi\Delta ft\right)| \ \ |\cos(2\pi\Delta ft) - \sin(6\pi\Delta ft)| \right) \mathrm{d}t = 0.6944 E_{\mathrm{s_{(elec)}}}. \tag{10}$$

By incorporating (10) into (9), the MSED between two IQFSK symbols can be evaluated as:

$$d^2_{\min} = 2E_{\mathrm{s_{(elec)}}} - 2\langle \boldsymbol{s}, \tilde{\boldsymbol{s}} \rangle_{\max} = 0.3056 \times 2E_{\mathrm{s_{(elec)}}}. \tag{11}$$

The MSED of other IQFSK counterparts is provided in Table I, which indicates that the MSED of IQFSK is lesser than other alternatives, implying a relatively poor performance. However, we accentuate that MSED is not the only parameter that impacts the overall performance, but it is also imperative to determine the number of symbol pairs that exhibit the MSED. Thus, we plot a histogram of $d^2/2E_{\mathrm{s_{(elec)}}}$ in Fig. 4 considering $M = 32$, which leads to $|\mathcal{D}| = 256$, from which we gather that less than 10% of
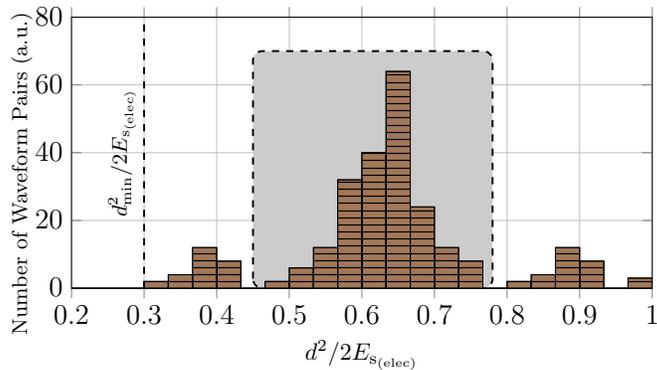
Fig. 4: Histogram of $d^2/2E_{s_{(elec)}}$ for IQFSK symbols considering $M = 32$.

the IQFSK symbols manifest a Euclidean distance closer to MSED. In contrast, most symbols embody a Euclidean distance much higher than MSED, as indicated by highlighted region of Fig. 4. Thus, it is foreseen that the MSED may not significantly impact the scheme's performance. This aspect shall become more apparent in the numerical simulation section, where we will perform the bit-error rate (BER) analysis and SE versus EE trade-off analysis.

C. Spectral Efficiency Analysis

IQFSK's four information-bearing elements are k_i, k_q, α_i, and α_q, which transmit $\{\lambda_i, \lambda_q\} = \log_2(M/4)$, $\{\lambda_{\alpha_i}, \lambda_{\alpha_q}\} = \log_2(2)$ bits, respectively. Thus, the total number of bits transmitted per IQFSK symbol of duration T_s is $\lambda = \lambda_i + \lambda_q + \lambda_{\alpha_i} + \lambda_{\alpha_q} = 2\log_2(M/2)$. Considering the bit rate, $R_b = \lambda/T_s$, and B, the SE of IQFSK, η is evaluated as:

$$\eta = \frac{R_b}{B} = \frac{4\log_2(M/2)}{M}. \tag{12}$$

The spectral efficiencies of the other alternatives are provided in Table I, where M is the DFT size. The maximum achievable SE of IQFSK is the highest as it effectively exploits independently the in-phase and the quadrature components in the symbol structure, which is not the case with other alternatives, as can be seen by the time transmit symbols, $s(t)$ of IQFSK counterparts in Table I.

IV. SIMULATION ANALYSIS OF IQFSK

This section evaluates IQFSK's performance through simulations and compares it to other FSK alternatives such as DCFSK, ACFSK, DCFPSK, and also to OOK. PPM's practical limitations (high PAPR) prevent it from being included in the comparison. The simulations consider DCFPSK with $M_\varphi = 4$ [8]. For the proof-of-concept, the simulations consider an additive white Gaussian noise (AWGN) channel as conventionally done in the literature. Moreover, it is established in [2] that impact of the time-dispersive
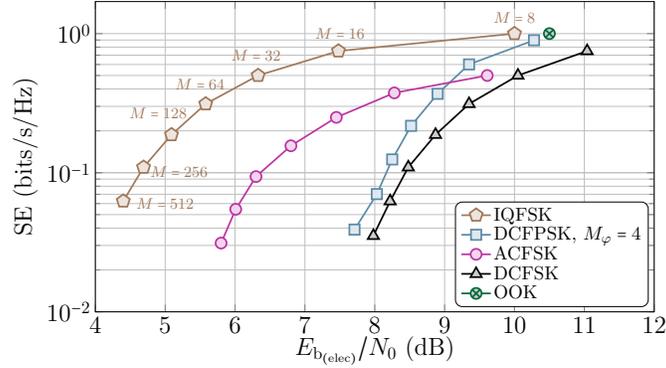
Fig. 5: SE/EE trade-off for IQFSK considering ML detection for a target BER of 10^{-3}. Here M is the size of DFT/DCT.

nature of the channel does not impact the performance of the schemes for low data rates. The metrics which we compare through simulations are SE and EE trade-off analysis and BER performance analysis. All the simulations involve 10^6 Monte Carlo runs. The simulation results are presented individually for each scheme's ML and sub-optimal detection mechanisms. The sub-optimal detection is equivalent to 1-tap detection in the frequency domain (refer to [2], [8], [9]).

A. Spectral Efficiency versus Energy Efficiency Analysis

Fig. 5 depicts the SE versus EE performance of IQFSK and other counterparts considering the ML detection mechanism. The SE is altered by varying $M = 2^i$ for $i = [\![3, 9]\!]$, whereas the EE for a given SE is attained by determining the electrical signal-to-noise ratio per bit, $E_{b_{(elec)}}/N_0$, required for achieving a BER of 10^{-3}. $E_{b_{(elec)}}/N_0$ is linked to $E_{s_{(elec)}}$ as $E_{b_{(elec)}}/N_0 = E_{s_{(elec)}}/N_0\lambda$. It is recalled that the required $E_{b_{(elec)}}/N_0$ reduces with an increase in M for all the FSK schemes. From Fig. 5, we can observe that SE versus EE performance depicted by IQFSK is the best among all the considered schemes in SE range of $[0.0625, 1]$ bits/s/Hz. For SE of 0.0625 bits/s/Hz (i.e., $M = 512$), there is a significant improvement of approximately 1.6 dB in favor of IQFSK relative to ACFSK. The performance of other alternatives considering ML detection, such as DCFSK, and DCFPSK with $M_\varphi = 4$, is inferior relative to the proposed scheme. Moreover, IQFSK with $M = 8$ performs marginally better than OOK when optimally detected. It is important to note that unlike the proposed scheme, OOK does offer SE versus EE trade-off. Thus, the superiority of IQFSK over other alternatives is apparent when the ML detection mechanism is considered.

Fig. 6 illustrates the SE versus EE comparison considering the sub-optimal detection mechanism. We can again observe that the performance of IQFSK is the best among all the considered approaches as it can achieve higher spectral efficiencies for a given required $E_{b_{(elec)}}/N_0$. In the case of sub-optimal detection as well, the performance of ACFSK is the closest to IQFSK's. We can observe that for $E_{b_{(elec)}}/N_0$ of approximately 6.4 dB, IQFSK exhibits a SE of 0.0625 bits/s/Hz (i.e., $M = 512$), while the SE of
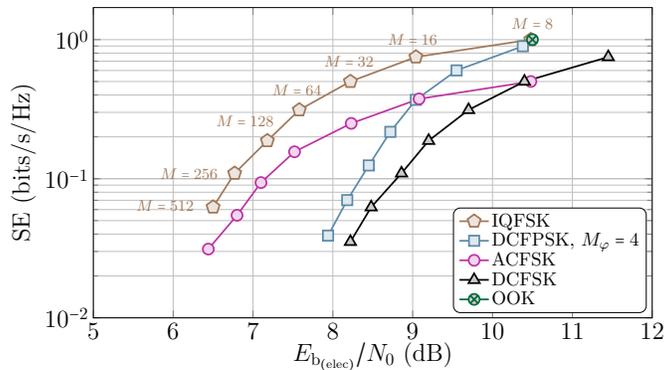
Fig. 6: SE/EE trade-off for IQFSK considering sub-optimal detection for a target BER of 10^{-3}. Here M is the size of DFT/DCT. ACFSK is 0.0312 bits/s/Hz ($M = 512$), exactly half of IQFSK. The sub-optimally detected IQFSK for $M = 8$ exhibit the same performance as OOK when optimally detected. The performance of IQFSK is better than other counterparts when considering sub-optimal detection.

B. Bit-Error Rate Analysis

In this section, we examine the BER performance of IQFSK using ML and sub-optimal detection mechanisms and compare it to other alternatives. Our benchmark SE for IQFSK is 0.1875 bits/s/Hz ($M = 128$), while the SEs closest to it for other options are 0.1250 bits/s/Hz for DCFPSK with $\{M, M_\varphi\} = \{256, 4\}$, 0.1562 bits/s/Hz ($M = 64$) for ACFSK, and 0.1875 bits/s/Hz for DCFSK. We also assess IQFSK's performance with SE of 0.1094 bits/s/Hz ($M = 256$) to illustrate how a decrease in SE permits to decrease in the BER for our proposed scheme, as most schemes have a lower SE than our benchmark. Moreover, the performance of OOK with optimal detection having SE of 1 bits/s/Hz is also provided and is also compared with IQFSK with SE of 1 bits/s/Hz ($M = 8$). Besides that, for 1 bits/s/Hz, the performance of IQFSK with ML detection is marginally better than OOK; IQFSK also offers flexibility in achieving different spectral and energy efficiencies by changing M, where the EE can be improved by increasing M.

Fig. 7 illustrates the BER performance of IQFSK considering ML detection. It can be observed that the BER performance of IQFSK is the best among all the considered approaches for the spectral efficiencies closest to the benchmark SE. The scheme whose performance is most comparable to the proposed one is ACFSK; however, for the same BER of 10^{-3}, ACFPSK requires 2 dB higher $E_{b_{(elec)}}/N_0$, and the SE is 17% lower. On the other hand, we also observe that DCFSK requires 4 dB higher $E_{b_{(elec)}}/N_0$ than the proposed schemes for the same SE. It is also evident that even with lower spectral efficiencies, the BER performance of DCFSK with $M_\varphi = 4$ and ACFSK is worse than the proposed approach.

Fig. 8 compares the BER performance of the proposed approach considering sub-optimal performance. We observe that the performance of IQFSK is still better than all the other schemes. In the case
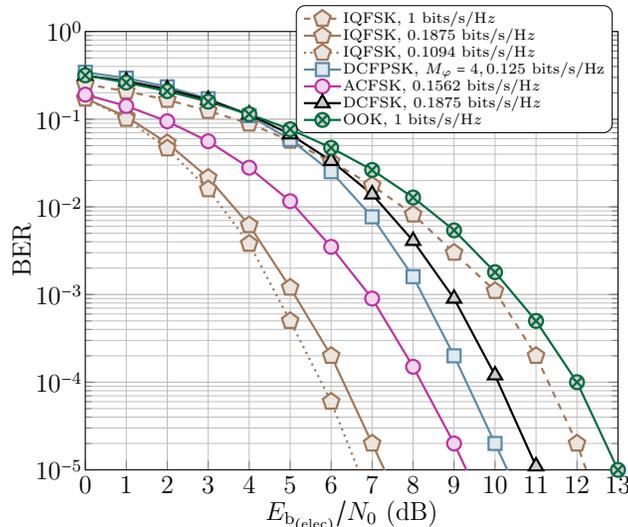
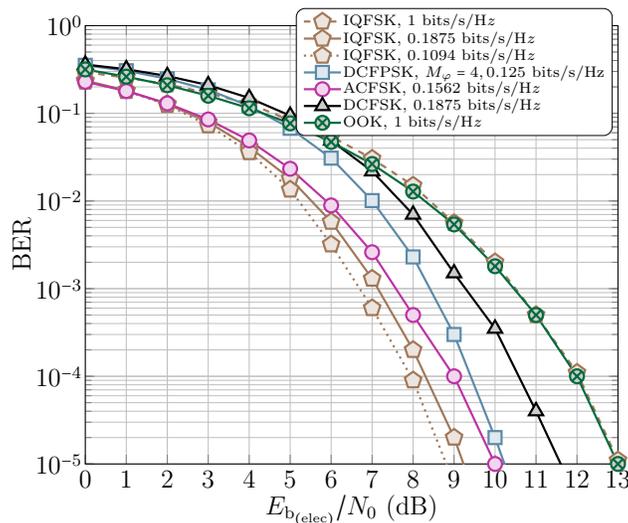Fig. 7: BER performance comparison considering ML detection.

Fig. 8: BER performance comparison considering sub-optimal detection.

of sub-optimal detection as well, the performance of ACFSK is closest to IQFSK's. ACFSK requires approximately 0.4 dB higher $E_{b_{(elec)}}/N_0$ than IQFSK while manifesting about 17% lower SE. We observe that for 1 bits/s/Hz, the performance of IQFSK with sub-optimal detection is equivalent to that of OOK employing an optimal detection mechanism. It is evident from Fig. 8 that the performance of IQFSK is better than all the other schemes considering sub-optimal detection as well.

V. CONCLUSIONS

In this work, we propose IQFSK scheme for low-power applications based on OWC. Unlike the state-of-the-art schemes, IQFSK fully exploits the in-phase and the quadrature components to augment the SE. The resultant waveform design is also efficient relative to other counterparts in terms of EE,

as depicted by BER performance and SE versus EE analysis considering both the ML and the low-complexity sub-optimal detection. Furthermore, we also analyze the Euclidean distance of the IQFSK symbols and gather that they are not orthogonal due to the clipping distortion induced due to zero-level clipping of the time domain symbol to make it coherent with IM-DD implementation. We also analytically determine the MSED for IQFSK waveforms. Even though IQFSK performs better in terms of SE and EE, its ML detection process is cumbersome. As M increases, the dictionary's cardinality for IQFSK becomes enormous, making the evaluation of the inner product between the received waveform and all the waveforms in the LUT a tedious task. It is foreseen that the highlighted benefits of the IQFSK waveform design would encourage further research, particularly in the development of low-complexity optimal detection mechanisms.

REFERENCES

[1] T. Maksymyuk, J. Gazda, B. Shubyn, O. Karpin, O. Kapshii, O. Urikova, E.-M Amhoud, M. Liyanage, M. Jo, and M. Dohler. Metaverse of Things in 6G Era: An Emerging Fusion of IoT, XR, Edge AI and Blockchain Technologies. In *Emerging Networking in the Digital Transformation Age: Approaches, Protocols, Platforms, Best Practices, and Energy Efficiency*, pages 546–564. Springer, 2023.

[2] A. W. Azim, A. Rullier, Y. Le Guennec, L. Ros, and G. Maury. Energy efficient M-ary frequency-shift keying-based modulation techniques for visible light communication. *IEEE Trans. Cogn. Commun. Netw.*, 5(4):1244–1256, 2019.

[3] H Park and J. R. Barry. Trellis-coded multiple-pulse-position modulation for wireless infrared communications. *IEEE Trans. Commun.*, 52(4):643–651, 2004.

[4] K. Kikuchi and M. Osaki. Highly-sensitive coherent optical detection of M-ary frequency-shift keying signal. *Opt. Express*, 19(26):B32–B39, 2011.

[5] S. Arnon. The effect of clock jitter in visible light communication applications. *IEEE/OSA J. Light. Technol.*, 30(21):3434–3439, 2012.

[6] S. He, G. Ren, Z. Zhong, and Y. Zhao. M-ary variable period modulation for indoor visible light communication system. *IEEE Commun. Lett.*, 17(7):1325–1328, 2013.

[7] E. Guler, C. Geldard, A. Baldwin, and W. Popoola. A demonstration of frequency-shift keying in underwater optical wireless communications. In *CLEO: QELS Fundamental Science*, pages JW3B–104. Optica Publishing Group, 2022.

[8] A. W. Azim, Y. Le Guennec, and L. Ros. Hybrid frequency and phase-shift keying modulation for energy efficient optical wireless systems. *IEEE Wire. Commun. Lett.*, 9(4):429–432, 2020.

[9] M. J. Khan, A. W. Azim, Y. Le Guennec, G. Maury, and L. Ros. Asymmetrically clipped-FSK modulation for energy efficient visible light communications. In *IEEE PIMRC*, pages 458–464, 2021.

[10] G.M. M. Yamga, A. R. Ndjiongue, and K. Ouahada. Low complexity clipped frequency shift keying (FSK) for visible light communications. In *2018 IEEE 7th International Conference on Adaptive Science & Technology*, pages 1–6. IEEE, 2018.

[11] M. L. G. Salmento, G. M. Soares, J. M. Alonso, and H. A.C. Braga. A dimmable offline LED driver with OOK-M-FSK modulation for VLC applications. *IEEE Transactions on Industrial Electronics*, 66(7):5220–5230, 2018.